

Structural relaxation and metal-insulator transition at the interface between SrTiO₃ and LaAlO₃

Natalia Pavlenko^{1,2} and Thilo Kopp¹

¹*EKM, Universität Augsburg, 86135 Augsburg, Germany*

²*Institute for Condensed Matter Physics, 79011 Lviv, Ukraine*

(Dated: November 21, 2018)

The electronic structure of interfaces between LaAlO₃ and SrTiO₃ is studied using local spin density approximation (LSDA) with intra-atomic Coulomb repulsion (LSDA+U). We find that the nature of the interface metallic states is strongly affected by the type of the structure (sandwich or bilayer) and by the termination surface of LaAlO₃. In all structures the atomic relaxation plays a crucial role in the electronic properties of the system. While in sandwiches the structural relaxation produces a significant polarization in SrTiO₃ and Jahn-Teller like splitting of Ti 3d_{xy} orbitals, in AlO₂-terminated bilayers the relaxation occurs primarily in LaAlO₃ and results in an insulator-metal transition which has been observed experimentally with increasing thickness of the LaAlO₃ layer.

PACS numbers: 74.81.-g,74.78.-w,73.20.-r,73.20.Mf

I. INTRODUCTION

Interfaces in complex transition metal oxide heterostructures can play an important role for their physical properties¹. This is especially important for heterostructures which contain nm-thick films deposited on structurally compatible substrate layers. The lattice mismatch and the charge polarity due to structural discontinuities at a film-substrate interface are the driving forces of interfacial reconstruction which changes dramatically the interface electronic state and possibly the physical behavior of the entire film.

The character of such a reconstruction can range from purely electronic to mixed electronic-lattice. The electronic reconstruction occurs through a compensation of the interface polarity by charge self-doping. In addition, the lattice relaxation can modify the band structure (Jahn-Teller like effect) and redistribute the charge between the electronic levels with consequent changes of the electronic properties of the system.

Besides the interface region, the film surfaces frequently undergo a surface reconstruction. For the surfaces of transition metal oxides, this reconstruction can be related to an electron depletion of *d*-orbitals accompanied by lattice contraction, a process observed on several surfaces like for instance at Pt(111)². The charge compensation at the surface can also proceed via a formation of oxygen vacancies which bring extra positive charge into the top layer. In both cases, the lattice relaxation and polarization plays a key role and leads to changes of chemical bonding and covalencies of surface ions^{3,4}.

An example of a film-substrate heterostructure, which exhibits a combination of surface and interface reconstruction, is a system of a LaAlO₃ film on top of a SrTiO₃ substrate. This bilayer attracted much attention recently due to the discovered transition between metallic and insulating properties⁵, possible interface magnetism⁶ and superconductivity⁷. Electrostatic tuning of the charge

carriers allows to switch between superconducting and insulating state⁸. A nanoscale control of the interfacial properties has been achieved⁹ and nanoelectronics has become feasible¹⁰.

In LaAlO₃-SrTiO₃-heterostructures, a several unit-cell thick LaAlO₃ (LAO) film is grown on a mm-thick SrTiO₃ (STO) substrate. Due to the extremely small thickness of the LAO film, the top surface states are almost directly coupled to the interface. This coupling leads to a new cooperative mechanism of reconstruction which involves both surface and interface electron states. As a consequence of such a combination, one may expect a strong dependence of the physical properties on the thickness of the LAO film. In fact, experiments⁵ with LAO-STO give clear evidence of an abrupt increase of the carrier concentration and conductivity in heterostructures with LaO-TiO₂ interfaces of *n*-type and AlO₂ termination of the LAO film. These abrupt changes have a character of a transition between insulating and metallic states which occurs upon an increase of the LAO-thickness above a critical value of 3 unit cells in the direction perpendicular to the interface. As the pure electronic compensation of the interface polarity would result in 0.5 electrons in the interfacial region and in metallic properties, the insulating character of the system with the ultrathin LAO film suggests that other reconstruction mechanisms, different from the purely electronic, play a dominant role.

In this work, we present the results of electronic structure calculations of LAO-STO superlattices. The structure of model superlattices contains the bilayers of LAO and STO with a slab of vacuum on top of the LAO layer, a structure which closely resembles the experimentally studied LAO-STO heterostructures. To understand better the surface reconstruction, we compare our results with calculations for a sandwich-type STO-LAO-STO superlattice where an LAO unit cell is directly connected to the TiO₂-terminated STO layers. In the analysis of the lattice degrees of freedom, we perform a full structural relaxation of the considered systems which includes the

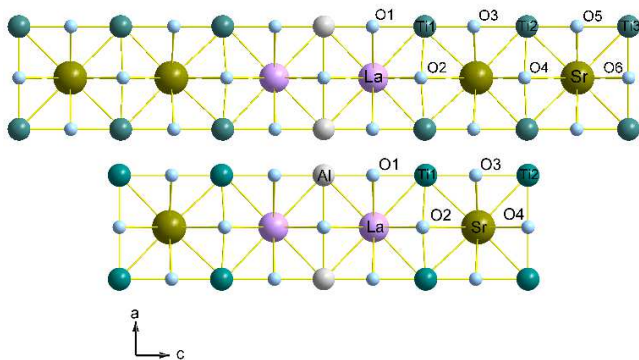


FIG. 1: Schematic view of relaxed LAO-STO sandwiches with $N_{\text{LaO}} = 2$ planes of LaO and $N_{\text{TiO}_2} = 2$ and 3 planes of TiO_2 in each substructure. Here, $N_{\text{TiO}_2} = 2$ for the bottom and $N_{\text{TiO}_2} = 3$ for the top structure, respectively. The distinct buckling in the interface TiO_2 planes is evident.

optimization of the lattice constants and of the atomic positions in supercells. In our calculations, we employ the SIC variant of LSDA+ U ^{11,12} on grids containing from $(8 \times 8 \times 1)$ to $(9 \times 9 \times 1)$ \mathbf{k} -points where the additional corrections due to Coulomb repulsion on $3d$ orbitals of Ti ($U_{\text{Ti}} = 2$ eV) and $5d$ orbitals of La ($U_{\text{La}} = 8$ eV) are included, according to estimates in Ref. 13.

As appears from our analysis of the TiO_2 -LaO interface stack, the reconstruction in STO-LAO-STO sandwiches differs from that in STO-LAO bilayers. The reason is the significance of the additional distortions in the near-surface planes of LAO in the bilayers, whereas in sandwiches we find only small atomic displacements in the interface LaO layers. Moreover, the reconstruction of STO-LAO bilayers depends on the type of surface termination of the LAO film. Below we consider the consequences of the surface termination. We will see that, despite similar TiO_2 -LaO interface stacking, the structural relaxation in all these systems leads to qualitatively different properties which demonstrates the key role of the lattice reconstruction.

II. INTERFACE RECONSTRUCTION IN SANDWICHES

It is well established in the literature³ that for the polar $(\text{LaO})^+-(\text{TiO}_2)^0$ interfaces, the “polar catastrophe” can be prevented by an electronic reconstruction mechanism¹⁴. In sandwiches LAO/STO/LAO/... with LAO terminated by a LaO plane (see Fig. 1), electronic reconstruction results in 0.5 electrons per interface unit cell required to maintain the overall neutrality of the system. It is remarkable that the negative “extra charge” is located mostly in the Ti $3d$ orbitals.^{15,16}

In the analysis of heterostructures which contain SrTiO_3 with its incipient ferroelectric properties, one also has to take into account the lattice degrees of freedom. Due to the high polarizability of the titanates, the charge

polarity at interface regions will inevitably induce local atomic distortions. The resulting atomic relaxations will modify the interface band structure and metallicity which can bring radical changes into the electronic reconstruction mechanism.

In the investigation of a combined electron-lattice reconstruction in LAO/STO, we first optimized the interface distance between TiO_2 and LaO layers within LDA¹¹. The optimal distance (1.89 Å) is shorter than the bond length [Ti-O] (1.953 Å) in bulk STO which implies a contraction of the interfacial TiO_6 octahedra in agreement with the results of Ref. 17. After this optimization at the interface, the local positions of atoms in the sandwich were relaxed to the new energetically favourable values. In each plane, the structural relaxation leads to significant, diametrically opposed displacements of Ti and O atoms in the [001] direction (denoted below by z). As a consequence, a static polarization is built up, characterized by the elongation of TiO_6 octahedra by about 0.1 Å in [001] direction and by a buckling of the TiO_2 planes. The changes of the length $\Delta_{AO} = z_A - z_O$ of each (A-O) bond (A = Ti, Sr, La) are shown in Fig. 2. These displacements cause a formation of static dipole moments in an initially paraelectric STO layer (similarly to what has been found in GGA and GGA+ U , Ref. 18) and reflect the degree of buckling of LaO, TiO_2 and SrO planes. A good convergence of the dipole moments within the interfacial region of 25 Å is achieved already for systems containing seven TiO_2 -planes in the supercell. The dependence of the displacements on the distance from the interface agrees well with the results of Ref. 19, which suggest an exponential decay of the displacements. The largest bond distortions of 0.15 Å appear in the TiO_2 planes and increase for increasing thickness of the STO layers. In contrast to the STO layer, the distortions in

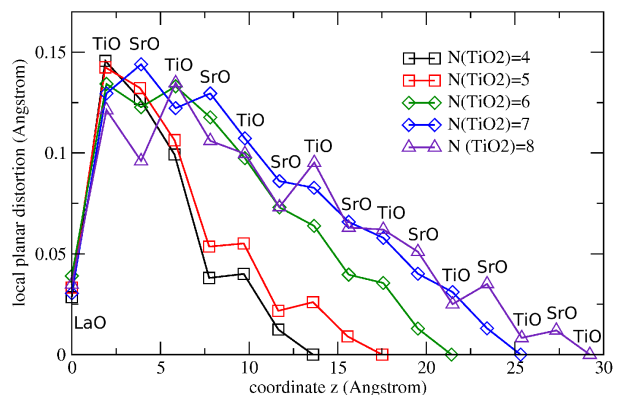


FIG. 2: Static dipole distortions in the planes SrO and TiO_2 which form with increasing number of STO unit cells in a periodic STO-LAO-STO supercell. The local planar distortions (vertical axis) are the changes of the length $\Delta_{AO} = z_A - z_O$ of each (A-O) bond (A = Ti, Sr, La) with respect to their bulk values. Here the coordinate z measures the distance from the interface LaO plane of the sandwich LAO/STO/LAO to each plane in STO.

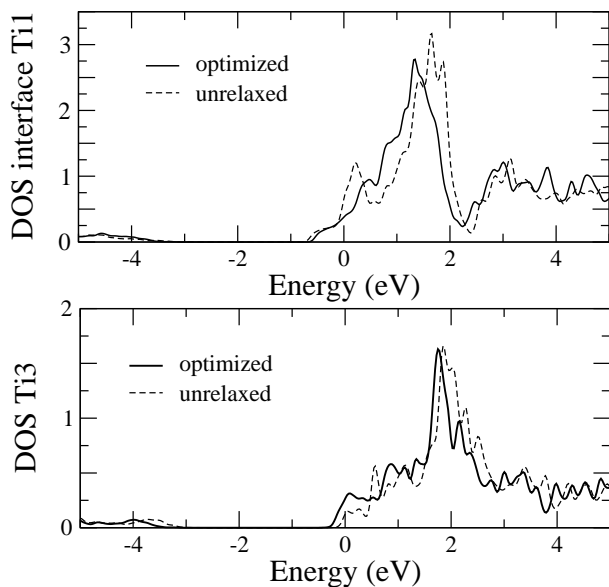


FIG. 3: Projected densities of states for Ti1 in the interface TiO_2 layer and for Ti3 in the TiO_2 plane separated by a distance $2a = 7.81 \text{ \AA}$ from the interface in a STO-LAO-STO sandwich with unrelaxed and optimized atomic positions ($N_{\text{TiO}_2} = 3$ and $N_{\text{LaO}} = 2$).

the LAO planes are negligibly small. It is worthwhile to note that the most significant atomic displacements $\Delta \geq 0.05 \text{ \AA}$ do not extend beyond a thickness of approximately 20 \AA , which measures an effective depth of structural relaxations near the interface.

In the electronic band structure calculated within LSDA+ U , the deformation of TiO_6 produces a Jahn-Teller splitting of t_{2g} states. It should be noted that the t_{2g} states are partially filled by the charge carriers appearing due to the electronic reconstruction of the polar

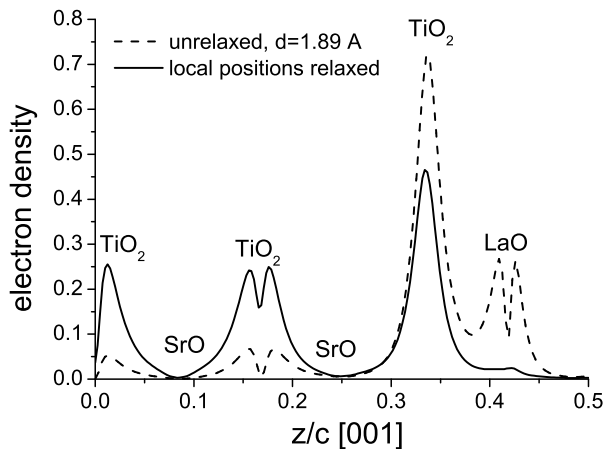


FIG. 4: Electron density profiles in structurally unrelaxed and optimized STO-LAO-STO sandwiches with $N_{\text{TiO}_2} = 3$ and $N_{\text{LaO}} = 2$. The density is determined from the integration over the density of states of Fig. 3.

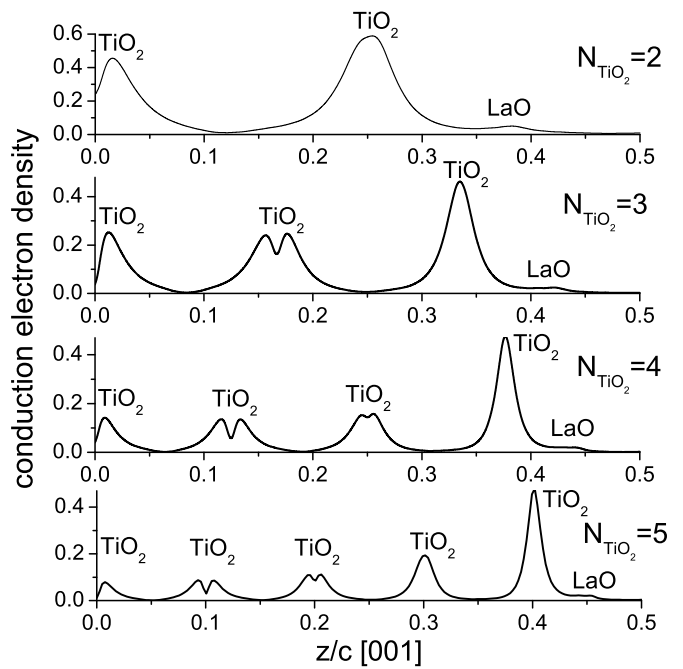


FIG. 5: Electron density profiles in structurally optimized STO-LAO-STO sandwiches with $N_{\text{LaO}} = 2$ for different N_{TiO_2} .

LaO-STO interface. Specifically, the structural distortions split the t_{2g} levels into d_{xy} and degenerate d_{xz} and d_{yz} bands. As the atomic displacements strongly depend on the distance from the interface, the level splitting and related changes in the band structure will be different in the interface region and in the layers more distant from the interface. Fig. 3 shows the modifications of the projected density of states of Ti in the layer next to the interface (Ti1) and in a more distant (3^{rd}) layer (Ti3). In the interface layer, the relaxation leads to a slight shift of the conduction $3d_{xy}$ band and, more prominently, to a reduced DOS close to the Fermi energy which suggests a decrease of the charge carrier density. In contrast to the interface TiO_2 , the relaxed $3d_{xy}$ band of Ti3 is displaced further below the Fermi level and the DOS at the Fermi energy is enhanced. The shifts of the conduction bands also produce changes in their respective occupancies. They can be calculated through the integration of the DOS in the range between the bottom of the conduction band and the Fermi level. The calculated profiles of the electron charge density (Fig. 4) suggest a charge depletion of the interfacial TiO_2 -LaO stack and consequent accumulation of the electron charge in the TiO_2 layers which are more distant from the interface.

The depletion of conducting charge in the interface layers not only results from the relaxation but may also be triggered through a growing number of TiO_2 planes in STO. This fact can be observed in Fig. 5 which demonstrates a redistribution of a fixed amount (0.5) of compensated charge with an increasing number N_{TiO_2} of

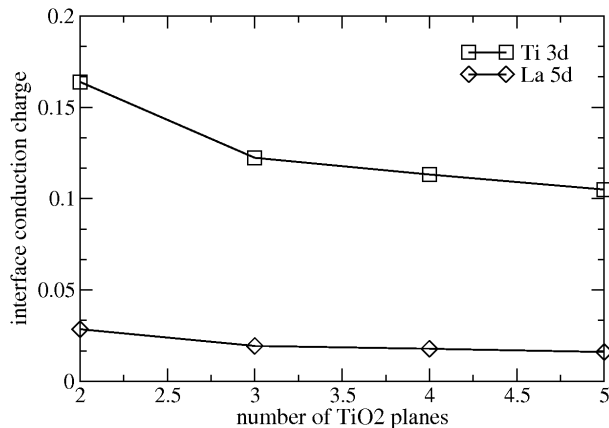


FIG. 6: Electron charge as a function of the number of TiO₂ planes in structurally optimized STO-LAO-STO sandwiches with $N_{\text{LaO}} = 2$.

TiO₂ layers from 2 to 5. An important consequence of the electronic reconstruction at the interface is a decrease of electron density in the TiO₂ and LaO interface planes (see Fig. 6) which is stronger in systems with wider STO substructure. In our calculations, an increase of the number of TiO₂ planes, N_{TiO_2} , leads to a decrease of charge in the interfacial TiO₂ plane, with a tendency for a saturation of electron charge in the interface TiO₂ plane to a value of about 0.1 electrons for a growing number of TiO₂ planes in the STO slab. In the STO layer with 5 TiO₂ planes, the residual 0.4 electrons are distributed within the more distant TiO₂ planes, but about 73% of the whole charge is located in the first three TiO₂ planes. It suggests a confinement of electron charge in an interface region of a thickness of 10–20 Å in the STO layer. This finding agrees well with the experimental distribution of the Ti excess charge discussed in Ref. 4, where the distinct peaks of the excess charge and its substantial decay with increasing distance from the interface demonstrate the confinement of charge to the interfacial region of a width of about 30 Å. Specifically, for sandwiches containing 9 to 11 TiO₂ layers, the Ti excess charge approaches a value slightly above 0.1 electrons at a distance of about 3–4 Å, an experimental value⁴ which is compatible with the values presented in Fig. 5.

We reason that the small width of the interfacial region is consistent with the conclusion that a quasi-two-dimensional electron gas is formed near the interface of a LAO-STO heterostructure with a mm-thick STO substrate (as discussed in Ref. 5 and, more recently, in Ref. 20).

III. ROLE OF SURFACE RECONSTRUCTION FOR THE ELECTRONIC PROPERTIES OF BILAYERS

Experimentally, it has been established that LAO-STO heterostructures with more than three unit cells of LAO

on STO substrates are metallic. For the analysis of the insulator-metal transition with increasing thickness of the LAO film, one has to account for the features inherent to surfaces of transition metals and their oxides. The current studies of these surfaces are motivated by drastic changes of their physical and chemical properties with the realization of different types of atomic reconstruction in the surface and subsurface layers. Furthermore, a number of *ab-initio* studies of this type of interfaces have identified a metallic *n*-type state with charge carriers which predominantly fill 3 d_{xy} orbitals.^{16,21}

Recent experiments give indications of a temperature dependence of the surface termination of LAO which changes from AlO₂ to LaO planes with an increase of temperature above 523 K.^{17,22,23} Therefore, to understand the interface reconstruction mechanism in ultrathin LAO films with an interference between surface and interface states, it is instructive to consider separately two possible types of the surface plane (AlO₂ and LaO) in STO-LAO bilayers.

For our theoretical studies, we have generated supercells which contain several LAO unit cells deposited on 1.5 SrTiO₃ unit cells. We have restricted calculations to structures with $N_{\text{TiO}_2} = 2$ due to clear indications of charge confinement to a few unit cells of STO found in the analysis of sandwiches (section II). To consider the surface properties, we have also introduced a 13 Å vacuum layer on top of LaAlO₃. The thickness of the LaAlO₃ film has been varied from 1 to 3 unit cells. In a system with the topmost plane LaO, an extra half of a LAO unit cell has been attached to the top of the LAO film.

The LSDA+*U* calculations result in a stable nonmagnetic state of the system. In this state, the electronic properties strongly depend on the structural relaxation which is controlled by the thickness of the LAO film in the slab. Specifically, in the LSDA+*U* calculations, the initially chosen configurations with nonzero magnetic moments and charge inhomogeneities rapidly decayed to zero magnetic moments and to equal charge for all Ti atoms in each TiO₂ plane which excludes the possibility for a decisive role of charge or magnetic order on the resultant electronic state.

A. AlO₂ termination

To study the bilayers STO-LAO with an AlO₂ plane at the top surface (Fig. 7), we have generated a number of supercells with N_{LaO} varying from 1 to 3 LAO unit cells. In these supercells, the structural optimization results in a structure with large opposite distortions of cations and anions in the LaO planes and only small atomic displacements in the STO substrate (see Fig. 7). Such a relaxation pattern is completely distinct from the systems with LaO termination which will be considered in the following section III B. The details of the structural changes are presented in Table I.

TABLE I: Atomic displacements (in Å) in the top planes of STO-LAO bilayers with an AlO_2 plane at the surface. Here the atomic displacements of the top La sites are defined as $\Delta z_{\text{La}} = z_{\text{La}} - z_{\text{La}}^0$ where z_{La}^0 is the planar unrelaxed coordinate, and of the oxygen sites as $\Delta z_{\text{O}} = z_{\text{O}} - z_{\text{O}}^0$. An additional index La or Al at $z_{\text{O}_{\text{La}/\text{Al}}}$ refers to the oxygen position in the La or Al planes, respectively. The atomic distortions in the top LaO plane are defined as $\Delta z_{\text{LaO}} = 3\Delta z_{\text{La}} - 2\Delta z_{\text{O}_{\text{La}}}$. The buckling of the surface is given by the atomic distortions in the top AlO_2 layer which are defined as $\Delta z_{\text{AlO}_2} = 4\Delta z_{\text{O}_{\text{Al}}} - 3\Delta z_{\text{Al}}$.

N_{LaO}	Δz_{La}	$\Delta z_{\text{O}_{\text{La}}}$	Δz_{LaO}	Δz_{Al}	$\Delta z_{\text{O}_{\text{Al}}}$	Δz_{AlO_2}
1	0.29	0.05	0.77	0.015	-0.02	-0.125
2	0.11	-0.07	0.46	-0.11	-0.13	-0.19
3	0.06	-0.09	0.36	-0.09	-0.09	-0.09

The first important feature is the strong buckling of the LaO planes where the relative [La-O] displacement $\Delta z_{\text{LaO}} = 3z_{\text{La}} - 2z_{\text{O}}$ approaches a maximal value of 0.77 Å in the structure with $N_{\text{LaO}} = 1$ (cf. Fig 7). This displacement parameter Δz_{LaO} is introduced so as to characterize the dipolar distortion of a LaO plane. For $N_{\text{LaO}} > 1$ the displacement parameter Δz_{LaO} is considerably reduced.

The second key property is a displacement of the top-most AlO_2 plane. It comprises significant inward displacements of both Al and oxygen towards the LaO plane and a consequent decrease of the distance between the

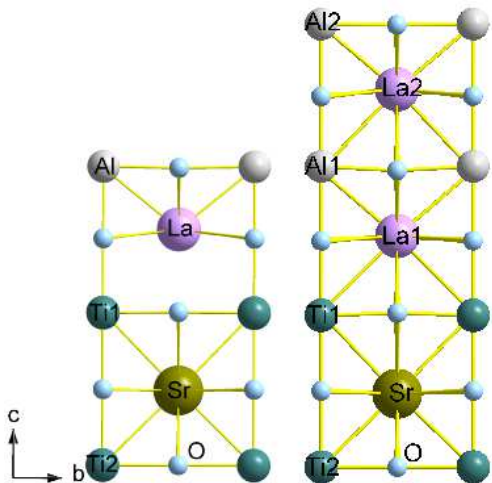


FIG. 7: Schematic view of relaxed LAO-STO heterostructures with $N_{\text{TiO}_2} = 2$ and with top layers of LaAlO_3 terminated by AlO_2 . Here the configurations with $N_{\text{LaO}} = 1$ and $N_{\text{LaO}} = 2$ are shown. For $N_{\text{LaO}} = 1$, the covalencies between La and the titanium and oxygen ions in the plane below are weak and no bonds are drawn. The full supercell for our calculations contains, apart from the vacuum cells, also the inverted structure so that the supercell geometry has two inversion symmetric interfaces and surfaces.

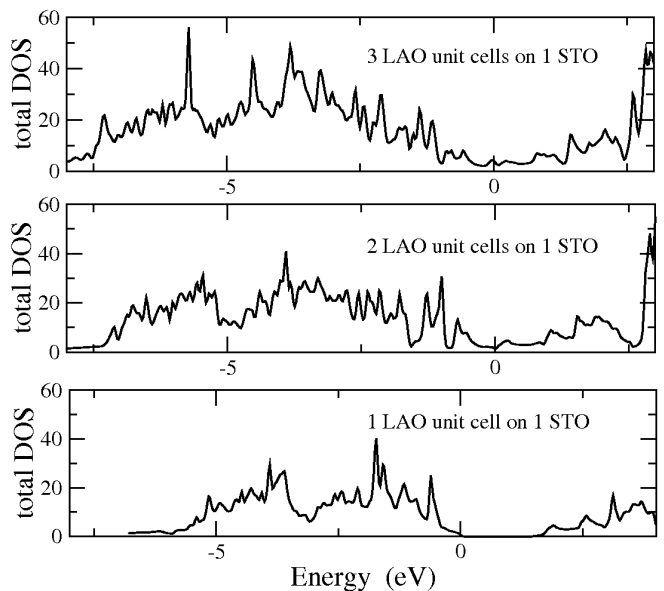


FIG. 8: Electron densities of states of a relaxed STO-LAO bilayer with an AlO_2 plane as the surface plane for $N_{\text{TiO}_2} = 2$ and different N_{LaO} .

AlO_2 plane at the surface and its adjacent LaO plane.

In the case of $N_{\text{LaO}} = 1$, the electric dipole moment, which is induced by the atomic distortions, is given by $\Delta P_{\text{LAO}} = \sum_i Q_i \Delta z_i$ where Q_i refers to the charge of the i -th site ($i = \text{Al}, \text{La}, \text{O}_{\text{Al}}, \text{O}_{\text{La}}$) where $\text{O}_{\text{Al}/\text{La}}$ is the oxygen in the AlO_2/LaO plane. One verifies that $\Delta P_{\text{LAO}} = Z_1 \Delta z_{\text{LaO}} + Z_2 \Delta z_{\text{AlO}_2} = 0.9 \text{ eÅ}$ where $Z_1 = -Z_2 = e$. Here, the displacement parameter for the AlO_2 plane is $\Delta z_{\text{AlO}_2} = 4\Delta z_{\text{O}_{\text{Al}}} - 3\Delta z_{\text{Al}}$.

On the other hand, the polar catastrophe in LAO²⁴ leads to the net electric polarization $P_{\text{LAO}}^0 = -ea_{\text{LAO}}/2 = -1.9 \text{ eÅ}$, where $a_{\text{LAO}} \simeq 3.8 \text{ Å}$ is the experimental bulk lattice constant of LaAlO_3 . While the interaction of electrons with the polarization P_{LAO}^0 tends to close the energy gap and stabilize the metallic state, the polarization due to atomic distortions is of opposite sign with respect to P_{LAO}^0 and leads to a competing tendency to stabilize the insulating state. In the monolayer LAO film with a dielectric constant ϵ , the interaction energy $E = eP_{\text{LAO}}/(4\pi\epsilon_0\epsilon a_{\text{LAO}}^2) \approx -1/\epsilon \text{ eV}$ of the total dipole moment $P_{\text{LAO}} = P_{\text{LAO}}^0 + \Delta P_{\text{LAO}} = -1 \text{ eÅ}$ with the electronic charge results in a reduced but finite energy gap of 1.5 eV which, for comparison, is approximately 4 eV in the LDA calculations of bulk LAO.

For the structure with $N_{\text{LaO}} = 2$, we have $P_{\text{LAO}}^0 = -N_{\text{LAO}}ea_{\text{LAO}}/2 = -3.8 \text{ eÅ}$ and $\Delta P_{\text{LAO}} = 0.65 \text{ eÅ}$. As a result, the increased net polarization $P_{\text{LAO}} = -3.15 \text{ eÅ}$ closes the energy gap and leads to the metallic state observed in Fig. 8.

In the densities of states in Fig. 8, the buildup of metallic states proceeds through the appearance of the electron carriers in the Ti $3d_{xy}$ bands which is exhibited in Fig. 10. This is accompanied by the filling of the gap which, for

$N_{\text{LaO}} = 1$, exists between the oxygen $2p$ and the La $5d$ and Ti $3d$ bands. The $2p$ states of the oxygens in the AlO_2 planes approach the Fermi energy from below and the interface Ti $3d_{xy}$ states cross the Fermi energy from above (see Fig. 9).

In experiments, STO-LAO bilayers with LAO films of $N_{\text{LaO}} = 3$ are still insulating whereas LAO films with $N_{\text{LaO}} \geq 4$ have been found to be metallic. In the present LDA-calculations, due to the underestimation of the energy gap by LDA, the “critical thickness” of the LAO layer is decreased by 2 and the metallic state occurs already at $N_{\text{LaO}} = 2$. Moreover, other localization effects may play a role in real materials^{25,26}, especially when the density of states at the Fermi energy is still small (cf. Fig. 9). In GGA calculations without lattice relaxation, the transition to a metallic state was identified for LAO films with $N_{\text{LaO}} = 4$ (supplement of Ref. 9). The GGA evaluation with lattice relaxation²⁷ produces a transition at around five monolayers of LAO.

Below the critical LAO-thickness, the polarity compensation via self charging (see Chap. II) reduces the energy gap, a process which however is partially suppressed due to structural distortions in the LAO layer. Similarly to the GGA results presented in Ref. 27, we can conclude here that the polarization in the LAO layer due to structural relaxation competes with the electric field caused by the polarity catastrophe and in this way establishes the insulating state in STO-LAO bilayers below the LAO critical thickness. In contrast, above the critical thickness the polarity compensation through the surface and interface charging leads to the metallic properties.

In the considered bilayers, two different charging processes can be distinguished which are exhibited by the composition of the density of states close to the Fermi energy (see the two panels of Fig. 9). Near the positively charged LaO layer at the TiO_2 -LaO interface, the com-

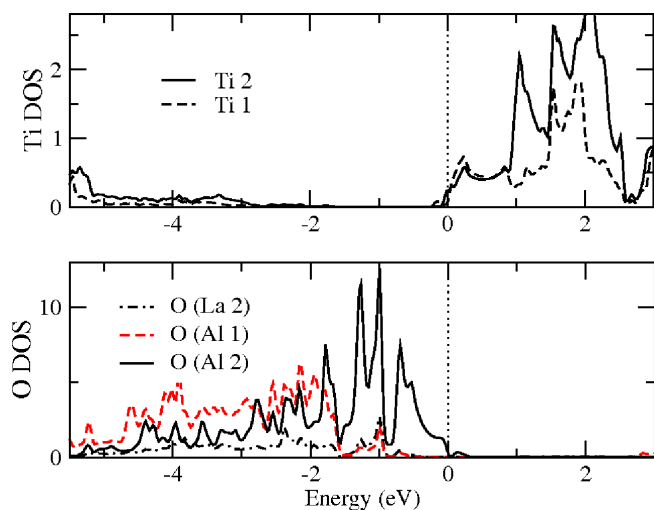


FIG. 9: Electron densities of states of Ti and oxygens in the LAO layer of a relaxed STO-LAO metallic bilayer with $N_{\text{TiO}_2} = 2$ and $N_{\text{LaO}} = 2$.

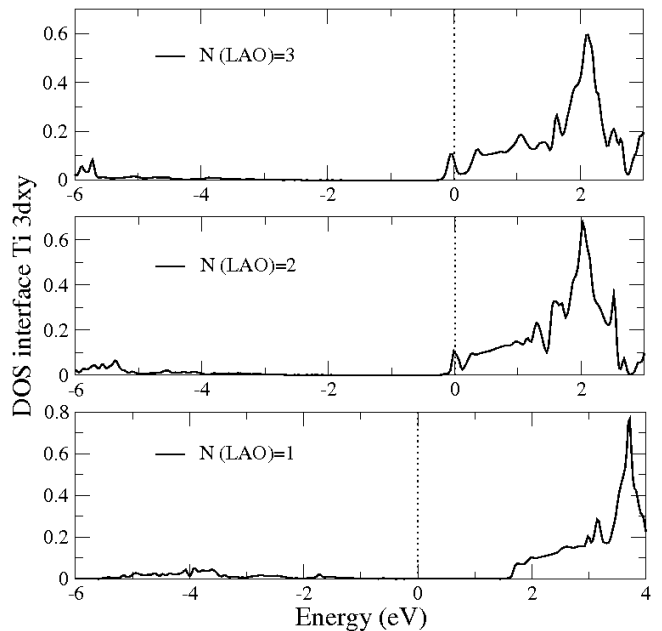


FIG. 10: Projected electron densities of states of the interface Ti $3d_{xy}$ orbitals for relaxed STO-LAO metallic bilayers with $N_{\text{TiO}_2} = 2$ and $N_{\text{LaO}} = 1, 2$ and 3 from bottom to top.

penetration produces the additional negative charge accumulated at Ti $3d_{xy}$ orbitals (see Fig. 9 and Fig. 10). In distinction to the interface, the negative polarity near the surface AlO_2 plane leads to additional holes distributed over the $2p$ orbitals of the surface oxygen which is clearly observed in the bottom part of Fig. 9. Recently, indirect indications for positive surface charge in STO-LAO have been discussed in Ref. 9 where such a positive surface charge is compensated by oxygen vacancies. In other experimental conditions, the surface hole charge can be also neutralized by surface oxidation or by near-surface bonding with negatively charged radicals which can be a possible reason for the insulating state usually found on the AlO_2 surfaces of LAO-STO bilayers.

B. LaO termination

The low- and room-temperature experiments are performed with heterostructures, in which the LAO films are terminated by AlO_2 planes in the case of TiO_2 -LaO interfaces. There are, however, several experimental indications of a transformation of the termination plane from AlO_2 to LaO, which occurs at temperatures around 423 K ^{17,22}. Such a transformation is explained through a formation of oxygen vacancies with simultaneous displacements of Al towards the subsurface layers. Although the discussed AlO_2 -LaO transformation remains still an open question, it is highly instructive to consider LaO terminated LAO films in the bilayers STO-LAO and to compare the electronic states with the electronic properties of AlO_2 terminated layers.

TABLE II: Structural parameters (in Å) for different N_{LaO} in STO-LAO bilayers with LaO termination. Here the atomic displacements of the top La sites are defined as $\Delta z_{\text{La}} = z_{\text{La}} - z_{\text{La}}^0$ where z_{La}^0 is the planar unrelaxed coordinate, and of the oxygen sites as $\Delta z_{\text{O}} = z_{\text{O}} - z_{\text{O}}^0$. The buckling of the surface is given by the atomic distortions of the top LaO bond $\Delta z_{\text{LaO}} = 3z_{\text{La}} - 2z_{\text{O}}$, and the length of the LaO-bond is denoted by Δ_{LaO} . The distance between the top LaO and the nearest subsurface plane is δ .

N_{LaO}	a	c	δ	Δz_{La}	Δz_{O}	Δz_{LaO}	Δ_{LaO}
2	3.805	32.17	1.8	-0.12	0.02	-0.4	2.7
3	3.755	39.75	1.85	-0.05	0.05	-0.25	2.69
4	3.759	47.32	1.85	-0.05	0.05	-0.25	2.66

For LaO termination at the topmost surface of the bilayers, we suggest and elaborate below that the reconstruction is controlled by the surface tensile stress which causes a charge occupation of $5d$ orbitals and a simultaneous contraction of the top surface layers².

In our supercells shown in Fig. 11, the thickness of the LaAlO_3 film has been varied from 1.5 to 3.5 unit cells whereas the thickness of the SrTiO_3 slab was fixed to 2 TiO_2 planes. In the heterostructure, the polar $(\text{LaO})^{+1}/\text{TiO}_2$ interface results in an effective electron doping by exactly one electron which is needed to achieve charge neutrality. In the context of the recent experiments^{5,6} the key question is the influence of the structural relaxation and the concomitant electronic reconstruction on the interface state, especially on its metallic and magnetic properties.

For the optimization of such supercells, we have performed a relaxation of the lattice constants $a = b$ in the

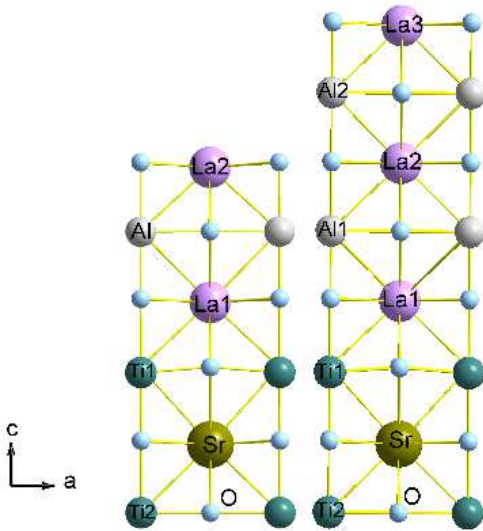


FIG. 11: Schematic view of relaxed LAO-STO heterostructures with $N_{\text{TiO}_2} = 2$ and with 1.5 and 2.5 top unit cells of LaAlO_3 ($N_{\text{LaO}} = 2$ and 3, respectively).

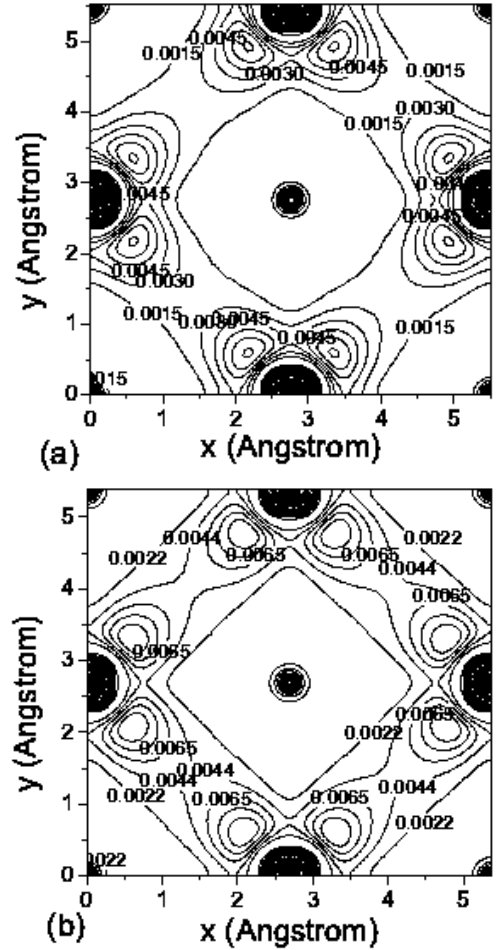


FIG. 12: Electron density map in the (x,y) plane of (a) unrelaxed and (b) optimized STO-LAO bilayer with $N_{\text{LaO}} = 2$ and $N_{\text{TiO}_2} = 2$. The coordinate $z/c = 0.29$ corresponds to the top surface LaO plane in the LAO film.

(x,y) plane and of the subsurface interplanar distances jointly with a further relaxation of the local atomic positions in the heterostructure. The results are presented in Table II. As appears in our calculations, the optimized planar lattice constant, a , strongly depends on the thickness of the LAO film, varying from 3.805 Å for $N_{\text{LaO}} = 2$ to 3.76 Å in a supercell with $N_{\text{LaO}} = 4$ which clearly shows a tendency to approach the bulk lattice constant for LaAlO_3 . It is worth noting that the volume LDA-optimization of bulk LaAlO_3 gives $a_{\text{LAO}}^{\text{LDA}} = 3.75 \text{ Å}$ which underestimates the experimental value $a_{\text{LAO}} = 3.789 \text{ Å}$. From Table II, one finds that already in ultrathin LAO films with $N_{\text{LaO}} = 3$ and $N_{\text{LaO}} = 4$ the planar lattice parameters a are sufficiently close to the bulk values.

In contrast to the sandwich-type structures characterized by small atomic displacements in the LAO film, in the considered bilayer the atomic relaxation leads (i) to a substantial change of the distances δ between the topmost LaO and nearest subsurface AlO_2 layers and (ii) to significant opposite displacements of the upper La and

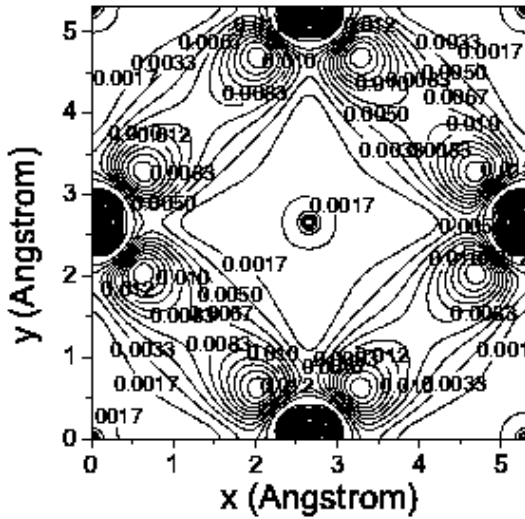


FIG. 13: Electron density map in the (x,y) plane of optimized LAO-STO bilayer with $N_{\text{LaO}} = 4$ and $N_{\text{TiO}_2} = 2$. The coordinate $z/c = 0.34$ corresponds to the top surface LaO plane in the LAO film.

oxygen atoms of the top LaO surface layers. Specifically, we find that the distance $[\text{LaO}-\text{AlO}_2]$ decreases by a value which ranges from 0.05 \AA in a system with $N_{\text{LaO}} = 4$ to 0.1 \AA for a structure with $N_{\text{LaO}} = 2$ (see Table II). Furthermore, for larger N_{LaO} the decrease of the La-O dipole moments in z direction and of the contraction of the planar lattice constant results in a shortening of length of the planar $[\text{La}-\text{O}]$ bond which varies from $\Delta_{\text{LaO}} = 2.7 \text{ \AA}$ for $N_{\text{LaO}} = 2$ to $\Delta_{\text{LaO}} = 2.66 \text{ \AA}$ for $N_{\text{LaO}} = 4$. We also note that in an unrelaxed heterostructure, where the lattice constant a is fixed to $a_{\text{STO}} = 3.905 \text{ \AA}$, the length of the $[\text{La}-\text{O}]$ bond is substantially longer than that of the relaxed system. To apprehend the role of the lattice and bond contraction for the electronic properties of the sub-surface layers, we performed LDA+ U calculations of the electronic structure of the generated optimized supercells for different values of N_{LaO} .

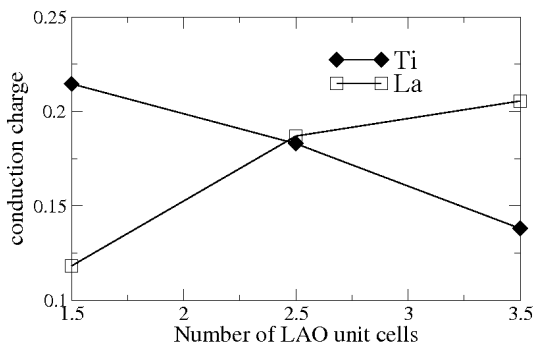


FIG. 14: Interface electron charge on La in the top LaO and on Ti in the interfacial TiO_2 planes for different numbers N_{LaO} of LAO planes in the heterostructure.

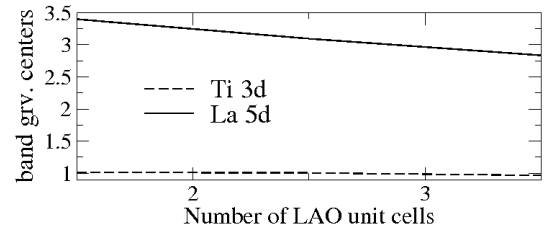


FIG. 15: Centers of gravity of top La $5d_{x^2-y^2}$ and interface Ti $3d_{xy}$ orbitals versus N_{LaO} .

As compared to the unrelaxed system, in a structure with a 1.5 unit-cell LAO film ($N_{\text{LaO}} = 2$) on SrTiO_3 , the Jahn-Teller like splitting due to atomic distortions leads to an increase of the gap between O $2p$ bands formed by oxygens in TiO_2 and LaO planes and mixed La $5d$ and Ti $3d$ states, an effect similar to that in the STO-LAO-STO-sandwiches. An opposite trend is obtained when we increase the thickness of the LAO film. Specifically, the thicker LAO layers exhibit smaller energy gaps and consequently higher charge carrier densities in the top LaO layer. The structural relaxation plays a central role for the modifications of the electronic structure. This is also illustrated in the charge density maps shown in Fig. 12(a) and Fig. 12(b).

In the unrelaxed structure with $N_{\text{LaO}} = 2$, more charge (about 0.6) is localized on La (Fig. 12(a)) of the topmost LaO layer. In the optimized system, the lattice contraction leads to a strengthening of covalent bonds and to a substantial carrier density which is distributed in the space between La and oxygen ions (Fig. 12(b)). In the optimized systems with $N_{\text{LaO}} \geq 3$, the increasing contraction results in a further increase of the charge density which is redistributed between La and O in the top LaO layer (Fig. 13). The obtained feature is closely related to the changes of the electron occupancy of top La and interfacial Ti shown in Fig. 14. As compared to the film with $N_{\text{LaO}} = 1$, in a thicker LAO film with $N_{\text{LaO}} = 3$ we find a transfer of the carrier density from the inter-

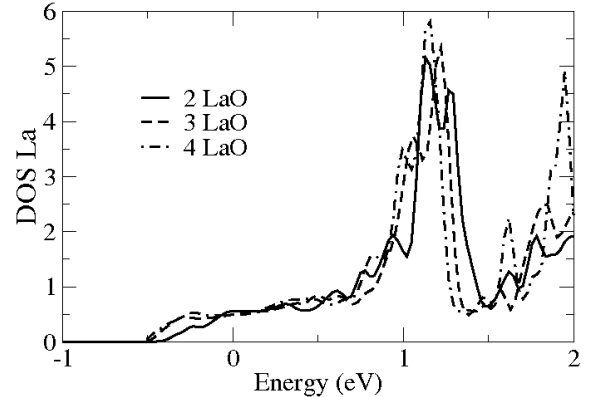


FIG. 16: Partial density of states of La in the top LaO plane for different N_{LaO} .

facial TiO_2 planes to the top LaO layers which appears due to the described structural transformations in subsurface layers. In Fig. 15 this Jahn Teller effect can be clearly detected by the strong decrease of the center of gravity of the $5d_{x^2-y^2}$ band of the top La which contrasts with the interfacial Ti $3d_{xy}$ band center that remains almost unchanged with the variation of the LAO thickness. Here a gravity center E_g of a band with a density of states $\rho(E)$ is calculated from the expression $E_g = \int dE E \rho(E) / \int dE \rho(E)$. The consequential increase of the electron charge on La (Fig. 14) is also related to the shift of the bottom of the La $5d_{x^2-y^2}$ band towards lower energies in Fig. 16 and is the direct result of the discussed electronic reconstruction.

IV. CONCLUSIONS

We have studied the electronic structure of interfaces between the bulk insulators LaAlO_3 and SrTiO_3 using the local spin density approximation (LSDA) with intra-atomic Coulomb repulsion (LSDA+ U). We find that the nature of the interface metallic states is strongly affected not only by the type (sandwich or bilayer) of the structure but also prominently by the termination surface of LaAlO_3 . In all types the atomic relaxation plays a crucial role for the electronic properties of the system.

In STO-LAO-STO sandwiches the structural relaxation results in an elongation of the TiO_6 octahedra by about 0.1 Å in the [001] direction and in a buckling of the TiO_2 planes of up to 0.15 Å for the plane nearest to the STO-LAO interface. These displacements cause a significant polarization in SrTiO_3 within about 10 Å from the interface. They also result in a Jahn-Teller splitting of the t_{2g} states and the interface charge resides mostly in the Ti $3d_{xy}$ bands. The conduction charge is confined essentially to the first three TiO_2 planes.

In bilayers the surface presents an additional important actor which may control the electronic state at the interface, especially when the surface is separated by an ultrathin film from the interface. For a LAO film on top of a STO substrate, the termination (either AlO_2 or LaO)

at the surface is crucial for the atomic relaxation and the electronic state at the LAO-STO interface.

In AlO_2 -terminated bilayers the relaxation occurs primarily in the LaAlO_3 film with minor displacements in SrTiO_3 . Specifically, the buckling of the subsurface LaO plane and the modified distances between the topmost (oppositely charged) AlO_2 and LaO planes introduces a polarization which decreases with the number N_{LaO} of LAO unit cells. For the unit cell thick LAO films, it is this lattice relaxation with the corresponding polarization of the film which counteracts the polarization introduced through the self charging (by 1/2 electron to compensate the interface polarity). For films with one unit cell LAO we identify an insulating state characterized by an energy gap of 1.5 eV between the Ti $3d_{xy}$ states of the TiO_2 plane next to the interface and the oxygen states of the topmost AlO_2 plane. For films with more than one unit cell LAO (i.e., $N_{\text{LaO}} > 1$) this gap closes due to the enhanced polarization from the self charging. Then the metallic state at the interface is formed by the Ti $3d_{xy}$ band with a finite density of states at the Fermi energy. This scheme results in a transition from insulating to metallic states: in the present LDA-calculations, due to the fact that LDA underestimates the gap, the metallic state occurs already at $N_{\text{LaO}} = 2$ whereas experiments show that bilayers with $N_{\text{LaO}} = 3$ are still insulating whereas LAO films with $N_{\text{LaO}} \geq 4$ have been found to be metallic.

Finally, for LaO-terminated bilayers the lattice relaxation is different: the surface tensile stress causes a charge occupation of La $5d$ orbitals and a corresponding contraction of the top surface layers. Here, one electron per interface unit cell is required to maintain the overall neutrality of the system. Both, the Ti $3d_{xy}$ states in the plane next to the interface and the La $5d_{x^2-y^2}$ have finite density of states at the Fermi energy and stay metallic, irrespective of the number unit cells in the LAO film.

We acknowledge helpful discussions with J. Mannhart and S. Thiel. This work was supported through the DFG SFB-484 and the TRR 80. Grants of computer time from the Leibniz-Rechenzentrum München through the HLRB project h1181 are gratefully acknowledged.

¹ E. Dagotto, *Science* **318**, 1076 (2007).

² V. Fiorentini, M. Methfessel, and M. Scheffler, *Phys. Rev. Lett.* **71**, 1051 (1993).

³ A. Ohtomo and H.Y. Hwang, *Nature* **427**, 423 (2004); *Nature* **441**, 120 (2006).

⁴ D.R. Hamann, D.A. Muller, and H.Y. Hwang, *Phys. Rev. B* **73**, 195403 (2006).

⁵ S. Thiel, G. Hammerl, A. Schmehl, C.W. Schneider, and J. Mannhart, *Science* **313**, 1942 (2006).

⁶ A. Brinkman *et al.*, *Nat. Mat.* **6**, 493 (2007).

⁷ N. Reyren *et al.*, *Science* **317**, 1196 (2007).

⁸ A.D. Caviglia *et al.*, *Nature* **456**, 624 (2008).

⁹ C. Cen, S. Thiel, G. Hammerl, C.W. Schneider, K.E. An-

dersen, C.S. Hellberg, J. Mannhart, and J. Levy, *Nature Materials* **7**, 298 (2008).

¹⁰ C. Cen, S. Thiel, J. Mannhart, and J. Levy, *Science* **323**, 1026 (2009).

¹¹ P. Blaha *et al.*, *WIEN2K, An Augmented Plane Wave + Local Orbitals Program for Calculating Crystal Properties*, ISBN 3-9501031-1-2 (TU Wien, Austria, 2001).

¹² V.I. Anisimov *et al.*, *Phys. Rev. B* **48**, 16929 (1993).

¹³ T. Bandyopadhyay and D.D. Sarma, *Phys. Rev. B* **39**, 3517 (1989).

¹⁴ This mechanism was demonstrated for a polar surface of K_3C_{60} by R. Hesper, L.H. Tjeng, A. Heeres, and G.A. Sawatzky, *Phys. Rev. B* **62**, 16046 (2000).

- ¹⁵ S. Gemming and G. Seifert, *Acta Mater.* **54**, 4299 (2006).
- ¹⁶ R. Pentcheva and W.E. Pickett, *Phys. Rev. B* **74**, 035112 (2006).
- ¹⁷ V. Vonk, M. Huijben, K.J.I. Driessen, P. Tinnemans, A. Brinkman, S. Harkema, and H. Graafsma, *Phys. Rev. B* **75**, 235417 (2007).
- ¹⁸ R. Pentcheva and W.E. Pickett, *Phys. Rev. B* **78**, 205106 (2008).
- ¹⁹ U. Schwingenschlögl and C. Schuster, *Chem. Phys. Lett.* **467**, 354 (2009).
- ²⁰ Sing *et al.*, arXiv/0809.1917, (2008).
- ²¹ U. Schwingenschlögl and C. Schuster, *Europhys. Lett.* **81**, 17007 (2008).
- ²² J. Yao, P.B. Merrill, S.S. Perry, and J.W. Rabalais, *J. Chem. Phys.* **108**, 1645 (1998).
- ²³ R.J. Francis, C.S. Moss, and A.J. Jacobson, *Phys. Rev. B* **64**, 235425 (2001).
- ²⁴ N. Nakagawa, H.Y. Hwang, and D.A. Muller, *Nature Materials* **5**, 204 (2006).
- ²⁵ S. Oh *et al.*, *Phys. Rev. B* **70**, 064509 (2004); J.N. Eckstein and I. Bozovic, *Annu. Rev. Mater. Sci.* **25**, 679 (1995).
- ²⁶ N. Pavlenko and T. Kopp, *Phys. Rev. B* **72**, 174516 (2005).
- ²⁷ R. Pentcheva and W.E. Pickett, *Phys. Rev. Lett.* **102**, 107602 (2009).